THE JOURNAL OF PHYSICAL CHEMISTRY A
A JOURNAL OF THE AMERICAN CHEMICAL SOCIETY

pubs.acs.org/JPCA

Article

Solvent-Mediated Charge Transfer Dynamics of a Model Brown Carbon Aerosol Chromophore: Photophysics of 1-Phenylpyrrole Induced by Water Solvation

Brianna N. Peterson, Megan E. Alfieri, David J. Hood, Christian D. Hettwer, Daniel V. Costantino, Daniel P. Tabor,* and Nathanael M. Kidwell*

Cite This: *J. Phys. Chem. A* 2022, 126, 4313−4325

Read Online

ACCESS | Metrics & More | Article Recommendations | Supporting Information

Downloaded via COLG OF WILLIAM & MARY on July 29, 2022 at 22:09:36 (UTC).
See https://pubs.acs.org/sharingguidelines for options on how to legitimately share published articles.

ABSTRACT: Nitrogen heterocycles are known to be important light-absorbing chromophores in a newly discovered class of aerosols, commonly referred to as "brown carbon" (BrC) aerosols. Due to their significant absorption and spectral overlap with the solar actinic flux, these BrC chromophores steer the physical and optical properties of aerosols. To model the local aqueous solvation environment surrounding BrC chromophores, we generated cold molecular complexes with water and a prototypical BrC chromophore, 1-phenylpyrrole (1PhPy), using supersonic jet-cooling and explored their intermolecular interactions using single-conformation spectroscopy. Herein, we utilized resonant two-photon ionization (R2PI) and UV holeburning (UV HB) double-resonance spectroscopies to obtain a molecular-level understanding of the role of water microsolvation in charge transfer upon photoexcitation of 1PhPy. Quantum chemical calculations and one-dimensional discrete variable representation simulations revealed insights into the charge transfer efficacy of 1PhPy with and without addition of a single water molecule. Taken together, our results indicate that the intermolecular interactions with water guide the geometry of 1PhPy to adopt a more twisted intramolecular charge transfer (TICT) configuration, thus facilitating charge transfer from the pyrrole donor to the phenyl ring acceptor. Furthermore, the water network surrounding 1PhPy reports on the charge transfer such that the H_2O solvent primarily interacts with the pyrrole ring donor in the ground state, whereas it preferentially interacts with the phenyl ring acceptor in the excited state. Large Franck−Condon activity is evident in the 1PhPy + $1H_2O$ excitation spectrum for the water-migration vibronic bands, supporting H_2O solvent reorganization upon excitation of the 1PhPy chromophore. Fluorescence measurements with increasing H_2O % volume corroborated our gas-phase studies by indicating that a polar water solvation environment stabilizes the TICT configuration of 1PhPy in the excited electronic state, from which emission is observed at a lower energy compared to the locally excited configuration.

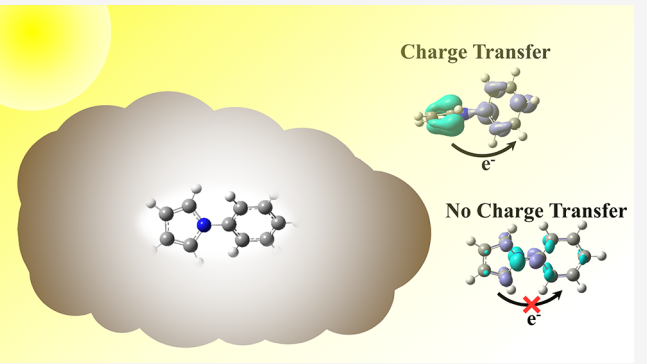

INTRODUCTION

Water-mediated interactions determine the structural, dynamical, and optical properties of aqueous solutions and interfaces,[1,2] which play a key role in biological folding,[3−5] photosynthetic energy conversion,[6−8] and aerosol solar absorption.[9−11] Considering the ubiquity of water-mediated interactions in numerous environments, there remain long-standing questions regarding how solvation shapes the photophysics of the solute partner. Thus, a fundamental description of the intermolecular interactions between the chromophore solute and H_2O solvent is still far from complete. The spatial configurations of solute-$(H_2O)_n$ molecular complexes offer exquisite insights not only into the nature of hydrogen-bonding forces that influence their stability, but they also serve as essential systems for understanding and modeling condensed-phase environments. In this view, molecular complexes act as a bridge between the gas and condensed phases.[12,13] The configurations of complexes provide a molecular-level understanding of solvation surrounding chromophore solutes in water networks that mimic air−liquid interfaces, leading to insights into their physical properties. Hydrogen-bonded molecular complexes occupy an interesting size regime large enough to exhibit significant complexity but small enough that their potential energy surfaces can still be explored in some detail by advanced experimental techniques and modern theoretical methods. Indeed, aerosol solar

Received: January 24, 2022
Revised: June 21, 2022
Published: July 1, 2022

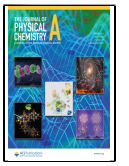

ACS Publications

© 2022 American Chemical Society

https://doi.org/10.1021/acs.jpca.2c00585
J. Phys. Chem. A 2022, 126, 4313−4325

absorption is steered by the photophysics and photochemistry of light-absorbing chromophores embedded within the aqueous environment of aerosols.

Aerosols are suspensions of fine liquid or solid particles in the atmosphere that impact public health, climate, and energy balance.[14] Carbonaceous aerosols are divided into distinct classifications depending on whether they are light-absorbing (black and brown carbon) or light-scattering (organic carbon).[15,16] Black carbon (BC) aerosol absorption does not vary with wavelength, whereas the absorption propensity of brown carbon (BrC) aerosols is highly dependent on wavelength with a smooth absorption increase from the visible to ultraviolet range.[17] BrC aerosols enhance light absorption and water evaporation that are key events to understanding the intricate relationships between clouds, aerosols, and global climate. The effects of clouds and aerosols are presently a major source of uncertainty in global climate and global atmospheric chemistry models.[18,19] In fact, it has been estimated[20] that BrC aerosols are responsible for up to 24% of radiative forcing that was previously thought to be from BC aerosols. Nitrogen heterocycles (N-heterocycles) have recently been identified as key light-absorbing chromophores in BrC aerosols.[21] Due to their significant absorption strengths and overlap with the solar flux, N-heterocycles shape the optical properties of BrC aerosols and global climate, even in low concentrations.

Pyrrole and pyrrole derivatives fulfill many of the common structural motifs identified as BrC chromophores.[21] There is also supporting evidence that intramolecular charge transfer (ICT) complexes may contribute to BrC aerosols due to their large transition dipole moment resulting in increased molar absorptivity.[22] 1-Phenylpyrrole (1PhPy) shown in Figure 1 is a model BrC chromophore and a plausible ICT molecule. Upon excitation of 1PhPy, electron charge transfer is initiated from the pyrrole π orbital donor to the phenyl ring π^* orbital acceptor. However, large-amplitude motion along the CN−CC torsional coordinate (highlighted in Figure 1) affects the degree to which charge transfer occurs. Electron donor/acceptor molecules can fluoresce from two relaxed singlet excited states (dual fluorescence). Upon photoexcitation, a locally excited state (LE) is formed, from which an ICT state with a larger dipole moment is generated. Dual fluorescence from electronic excitation of 1PhPy has been observed in nonpolar and polar solvents.[23,24] The two fluorescence bands have been attributed to radiative emission from an LE-state configuration obtained at various dihedral angles, whereas a perpendicular (CN−CC dihedral = 90°) geometry, often referred to as a twisted intramolecular charge transfer (TICT) configuration, is responsible for the red-shifted emission band. Polar solvents such as water may therefore stabilize the TICT geometry and the charge distribution following photoexcitation. In a twofold rotation scheme, a CN−CC dihedral angles of 0 and ±90° are regarded as having planar and perpendicular geometries, respectively, with barriers for torsional interconversion, ΔE_0 and ΔE_{90}.

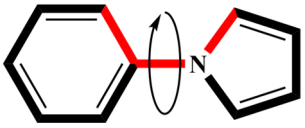

Figure 1. Structure of 1PhPy with the dihedral angle of interest highlighted.

Previous works have characterized the extent to which 1PhPy undergoes isomerization in the excited state from the LE geometry to the TICT structure. Okuyama et al.[25] recorded the ground- and excited-state vibronic spectra of the bare 1PhPy chromophore under jet-cooled conditions and fit the data with a Franck−Condon simulation analysis to determine the two torsional potential energy surfaces. Since the simulations yielded ΔE_{90} that was larger than ΔE_0 in the excited state, the authors concluded that 1PhPy does not adopt a perpendicular TICT geometry. Thomas et al. obtained the rotationally resolved spectrum of isolated 1PhPy in a molecular beam under an applied electric field and complemented experiments with calculations at the M05-2X/6-31G level of theory.[26] Their study found that the permanent electric dipole moment in the more planar ^1L_b excited state is reversed from the ground state, with the $\Delta\mu \sim 2.5$ D resulting from ∼0.15 e^- charge transfer from the pyrrole to the phenyl ring upon excitation. Carrying out theoretical calculations at the CASSCF/CASPT2 level of theory, Proppe and co-workers[27] determined that when 1PhPy is placed in acetonitrile solvent, ΔE_{90} is reduced, thus preferring a TICT geometry from which emission occurs at approximately 3.72 eV. In a follow-up study,[28] Manz utilized nonequilibrium molecular dynamics simulations to study the dynamics of 1PhPy in acetonitrile solvent and concluded that the TICT isomerization occurred on a 5−10 ps timescale, with rapid acetonitrile solvent reorganization on the order of 100 fs. More recently, the absorption and fluorescence of 1PhPy in the gas phase and in acetonitrile were carried out by Aguilar et al. at the CASPT2//CASSCF level, where they identified a stabilized TICT conformation in acetonitrile with a very flat free energy surface.[29] Furthermore, Schweke et al.[30] generated 1PhPy + acetonitrile complexes in an argon matrix and determined that 1PhPy behaved with TICT character as a complex.

The focus of this article is to determine the structural details of the charge transfer mechanism of 1PhPy in the absence and presence of water as a polar solvent to mimic the aqueous environment of BrC aerosols. Using mass-resolved spectroscopy and double-resonance methods in tandem with theoretical calculations, the intermolecular interactions of 1PhPy with water were investigated. Our goal is to reveal the role of water in shaping the charge transfer mechanism induced by electronic excitation of 1PhPy and whether a TICT spatial configuration is preferred in the hydrogen-bond network with water. Therefore, we aim to investigate these fundamental processes from the bottom-up to further understand the solar absorption outcomes of BrC chromophores and to model the local solvation environment surrounding BrC chromophores found in aerosols. Interpretation of the experimental spectra is aided by modeling the spectra from the energies and torsional wavefunctions calculated via discrete variable representation (DVR) calculations on the torsional potential energy surface. The DVR family of methods is useful for calculating the energies of arbitrary low-dimensional potentials, as the methods can be numerically converged by reducing the grid spacing. Fluorescence emission measurements recorded with increasing H_2O % volume report on the intramolecular charge transfer dynamics of 1PhPy in the condensed phase, translating more directly to the solar absorption outcomes of BrC aerosols.

https://doi.org/10.1021/acs.jpca.2c00585
J. Phys. Chem. A 2022, 126, 4313−4325

EXPERIMENTAL METHODS

1-Phenylpyrrole (1PhPy) was purchased from Sigma-Aldrich (99%) and used without further purification. All experiments were carried out in a custom-built chamber described previously.[31] 1PhPy was placed into a stainless-steel reservoir behind a 500 μm pulse valve nozzle (series 9 general valve) operating at 10 Hz and heated to 40 °C to obtain sufficient vapor pressure. The entire gas manifold is composed of two independent gas channels, wherein a single gas line containing helium (He; ca. 2−3 bar backing pressure) is split into a pure He gas channel to entrain the 1PhPy sample and another channel containing a reservoir with water to seed into the gas expansion. The two channels reconverge prior to the 1PhPy sample container. Water complexes with 1PhPy were selectively generated by opening a gas shutoff valve to the water gas channel, and the gas flow was fine-tuned with a needle valve to optimize experimental conditions. Using a mass flow meter (Teledyne Hastings), the 1PhPy sample gas flow, water gas flow, and total gas flow were monitored to determine molecular number densities (∼0.05% water). The gas mixture with or without water present was pulsed into a high-vacuum time-of-flight mass spectrometer, creating a molecular beam and adiabatically cooling 1PhPy or 1PhPy + $n$$H_2O$ complexes to their respective zero-point vibrational levels by supersonic jet expansion. A skimmer (2 mm; beam dynamics) was placed at a distance of 30 mm from the pulse nozzle to select the molecules or complexes with the lowest internal energy prior to laser interrogation.

In the collision-free region of the expansion downstream, the skimmed molecular beam is probed with resonant two-photon ionization (R2PI) spectroscopy to obtain vibrationally resolved excitation spectra out of the ground-state zero-point level with mass selectivity. Tunable ultraviolet (UV) light was generated by frequency-doubling the output of a Nd:YAG pumped dye laser (Radiant Dyes NarrowScan) with an Inrad Autotracker III equipped with a beta barium borate (BBO) crystal. The excited-state spectra were obtained by UV exciting 1PhPy or 1PhPy + 1H_2O to vibronic levels with the probe laser (10 Hz), from which the excited-state population was ionized using the same UV light source. The mass ion signal was gated and monitored as a function of the probe UV wavelength to generate the R2PI spectrum. While obtaining the R2PI spectra, we ensured that the transition intensities were not saturated using ∼0.2 mJ/pulse UV power. Therefore, the intensities represent the true absorption intensities for each transition band.

The R2PI spectrum is frequently the sum of contributions arising from multiple conformational isomers or fragments from photoionization of molecular complexes, which can be deconvoluted using ultraviolet holeburning (UV HB) double-resonance spectroscopy. Here, a holeburn laser (5 Hz) is spatially overlapped with the probe laser from the R2PI method and precedes the probe laser by 50 ns. The holeburn laser was fixed on and partially saturated specific vibronic features in the R2PI spectra due to a conformational or complex isomer, thus removing a sizeable fraction of the ground-state population. As the probe laser is scanned and becomes resonant with a shared ground-state transition as the holeburn laser, the isomer ground-state population is depleted. A difference spectrum is obtained by monitoring the gated mass ion probe signal using active baseline subtraction and averaging the signal depletion with the probe wavelength.

Next, condensed-phase fluorescence emission and excitation measurements of 1PhPy in varying solvent concentrations were obtained. Standard solutions of varying polarity were prepared using tetrahydrofuran (Fisher-Scientific, 100%) and ultra-pure water. Solutions were made in the % volume ratios of THF/H_2O of 100:0, 80:20, 60:40, 40:60, and 20:80. Approximately 0.016 g of 1PhPy was placed into individual 20 mL glass vials with each designated for a % volume ratio. Using a micropipette, 10 mL of the % volume solution was placed into each vial to dissolve the 1PhPy. The 20:80 sample was diluted to a concentration of approximately 0.00035 g/mL for full solvation. Fluorescence emission and excitation spectra were obtained using a Cary Eclipse Fluorescence Spectrophotometer (G9800A), whereby approximately 1 mL of the % volume sample solution was placed into a 1 cm quartz cuvette for analysis. Excitation spectra were obtained in the range of 190−325 nm with an emission wavelength of 330 nm, and emission spectra were obtained in the range of 285−800 nm with an excitation wavelength of 280 nm. The excitation and emission slit widths were 5 nm, and the scan resolution was 1 nm. A series of 3 scans were taken for each sample and then averaged.

COMPUTATIONAL METHODS

Quantum Chemical Calculations. All quantum chemical calculations were performed using the Gaussian16 suite.[32] The different conformers of 1PhPy were constructed by rotating the C−N dihedral bond between the pyrrole and phenyl aromatic rings shown in Figure 1. Ground-state vibrational frequency and optimization calculations were carried out using density functional theory (DFT), specifically the ωB97X-D level of theory with the 6-311G++(d,p) basis set.[33,34] The ωB97X-D functional has been used in previous studies considering its effectiveness at describing dispersive interactions between molecules as well as increasing long-range exact exchange, which removes long-range self-interactions. This allows for a more reliable modeling of charge transfer compared to other functionals.[35] Analogous excited-state calculations were carried out at the TD-DFT ωB97X-D/6-311G++(d,p) level of theory.

To search for the lowest-energy structures of the 1PhPy + $n$$H_2O$ complexes, the ABCluster program[36] was employed to generate initial guess structures. The configurational search identified global and local minima of molecular complexes using the artificial bee colony (ABC) algorithm, and all possible 1PhPy + $n$$H_2O$ (n = 1−3) complex isomers were obtained within a 50 kJ/mol energy window. Further geometry optimizations and harmonic frequency calculations were performed at the same levels of theory described for 1PhPy, and the lowest-energy isomers were identified. Vertical excitation calculations for 1PhPy and 1PhPy + $n$$H_2O$ (n = 1−3) were calculated for all optimized structures using TD-DFT ωB97X-D/6-311++G(d,p). Relaxed potential energy scans along the C−N dihedral angle were generated for 1PhPy and 1PhPy + $n$$H_2O$ (n = 1−2) in the ground and excited states using the same levels of theory as the geometry optimization calculations. The 6-31G++(d,p) basis set was used for the 1PhPy + 3H_2O dihedral scan in the excited state due to computational costs. The dihedral angle was scanned in 10° increments, and the relative energies were recorded to predict barriers to planarity (ΔE_0) and perpendicularity (ΔE_{90}). Where necessary, the potential energy scans were also carried out at 5 and 1° increments to investigate any

https://doi.org/10.1021/acs.jpca.2c00585
J. Phys. Chem. A 2022, 126, 4313−4325

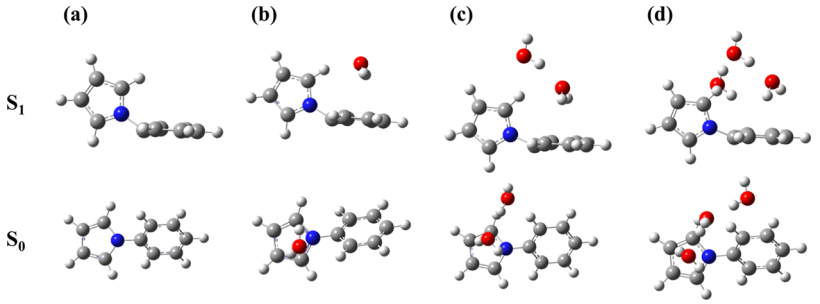

Figure 2. Optimized geometries of (a) 1PhPy, (b) 1PhPy + $1H_2O$, (c) 1PhPy + $2H_2O$, and (d) 1PhPy + $3H_2O$ in the ground (bottom) and excited (top) singlet electronic states at the ωB97X-D/6-311G++(d,p) and TD-DFT ωB97X-D/6-311G++(d,p) levels of theory, respectively.

effects that the additional resolution would have on the potential energy fitting procedure.

Discrete Variable Simulation of the 1PhPy and 1PhPy + H_2O Vibronic Spectra. The vibronic spectra of 1PhPy and 1PhPy + H_2O were simulated with periodic one-dimensional discrete variable representation (1D DVR) calculations.[37] The formulation of the potential and kinetic energy matrices follow the methods of Colbert and Miller.[38] For the potential energy, torsional potential energy scans were fitted on the ground and excited states for both 1PhPy and 1PhPy + $1H_2O$. Here, the torsional coordinate is defined as the average of the four CN−CC dihedral angles. Two interpolation schemes were employed in initial testing: cubic spline and linear interpolation, both constrained to periodic fits. Though the DVR method is a grid-based method, it is desirable to keep the potentials smooth (or analytic), and thus the periodic cubic spline is used for the results in this paper.

In the 1D DVR calculations of the torsional energy levels and wavefunctions, 1001 grid points were used (2001 grid points were used to test for convergence). The relative intensities of transitions between ground-state torsional wavefunctions found on each surface were taken to be the square of the absolute value of the overlap integral (evaluated over the discrete grid points) between the two wavefunctions, and the intensities were normalized to the largest square overlap. The following empirical parameters were added to finish fitting the spectra on top of this simplified model: (1) the position (in frequency) of the origin of the progression, (2) the effective mass (moment of inertia) of the torsion, (3) the starting point for the second progression with the same spacing (which appears to be due to a second vibrational mode), (4) for the 1PhPy + $1H_2O$ spectrum, a cutoff for the spectral progression is set to 350 cm^{-1}, and (5) the relative intensity of the second progression. The DVR code and supplemental code for generating the estimated spectra are provided on GitHub: (https://github.com/Tabor-Research-Group/phenylpyrole-dvr).

RESULTS

Computational Results. Figure 2 shows the optimized geometries for 1PhPy in the ground and excited electronic states. Only one conformer was found in the ground state with a CN−CC dihedral angle of 40.2°, which is a somewhat twisted configuration between complete planarity (0°) and complete perpendicularity (90°). By comparison, two different minima were found in the excited state, in which the lowest-energy conformation has a dihedral angle of 67.9° that is closer to perpendicularity. Relative to the ground-state geometry, the lowest-energy TICT isomer in the excited state has a bent structure with the pyrrole C−H bond oriented toward the phenyl ring. The NCC angle is 35°; here, we define the NCC angle as the difference between 180° and the angle between the pyrrole nitrogen atom and the phenyl ring carbon atoms at positions 1 and 4. The higher-energy locally excited (LE) geometry with a dihedral angle = 23.3° and an NCC angle ∼0° is less stable than the excited-state global minimum by approximately 300 cm^{-1}. Both excited-state geometries have previously been reported at the CASPT2//CASSCF level in the gas phase and in acetonitrile solution.[29] Tables 1 and 2 tabulate the geometrical parameters of 1PhPy in the ground and excited electronic states.

Table 1. Geometrical Parameters of the 1-Phenylpyrrole Optimized Structures with and without Water in the Ground Electronic State[a]

	1PhPy	1PhPy + $1H_2O$	1PhPy + $2H_2O$	1PhPy + $3H_2O$
dihedral (deg)	40.2	−54.2	40.1	44.5
NCC angle (deg)	0	0	0	1
N−C bond length (Å)	1.41	1.42	1.42	1.42

[a]Geometries optimized at the ωB97X-D/6-311G++(d,p) level.

Table 2. Geometrical Parameters of the 1-Phenylpyrrole Optimized Structures with and without Water in the First Excited Electronic State[a]

	1PhPy	1PhPy + $1H_2O$	1PhPy + $2H_2O$	1PhPy + $3H_2O$
dihedral (deg)	67.9	70.3	74.1	91.2
NCC angle (deg)	35	29	25	23
N−C bond length (Å)	1.48	1.47	1.46	1.45

[a]Geometries optimized at the TD-DFT ωB97X-D/6-311G++(d,p) level.

Figure 2 also shows the calculated geometries in the ground and excited electronic states for the 1PhPy + $1H_2O$, 1PhPy + $2H_2O$, and 1PhPy + $3H_2O$ complexes; Tables 1 and 2 list the relevant parameters of 1PhPy + nH_2O in both electronic states. Upon excitation, the dihedral angle changes from a semitwisted conformation in the ground state (−54.2, 40.1, and 44.5°) for 1PhPy + $1H_2O$, 1PhPy + $2H_2O$, and 1PhPy + $3H_2O$, respectively, to a more perpendicular conformation in the excited state (70.3, 74.1, 91.2°). Furthermore, the NCC angle for 1PhPy + $1H_2O$, 1PhPy + $2H_2O$, and 1PhPy + $3H_2O$, respectively, in the excited state is 29, 25, and 23°. The excited-

https://doi.org/10.1021/acs.jpca.2c00585
J. Phys. Chem. A 2022, 126, 4313−4325

state geometry of the 1PhPy solute within the water-complexed structures is similar to the bare 1PhPy chromophore such that the CH bond of the pyrrole ring orients toward the phenyl ring. Indeed, Figure 2 shows that 1PhPy adopts a bent structure upon excitation with a dihedral angle that increasingly approaches perpendicularity with the number of water molecules in the complex. A similar geometry of the 1PhPy chromophore in acetonitrile solvent has been reported in a previous theoretical study.[29] Calculations indicate that the $S_1 \leftarrow S_0$ adiabatic excitation energy decreases with sequential water addition relative to the bare 1PhPy chromophore and that the transition is consistent with a $\pi\pi^*$ excitation. Furthermore, higher-lying excited electronic states are not predicted to be close in energy to the first excited electronic state. As seen in the figure for 1PhPy + $1H_2O$, water prefers to bind with the pyrrole ring in the ground electronic state through a hydrogen atom-π interaction. However, upon excitation, this interaction changes with the water now bridging the two rings as both a hydrogen atom acceptor with the pyrrole ring and a donor to the π^* orbital localized on the phenyl ring. The 1PhPy + nH_2O (n = 2, 3) complexes demonstrate similar ground- and excited-state interactions as the singly solvated complex, with the water network fully extending between the pyrrole and phenyl π-systems for 1PhPy + $3H_2O$.

As observed in the ground-state dihedral potential energy scan shown in Figure 9a, 1PhPy has clear barriers to planarity (ΔE_0; dihedral angle = 0°) and perpendicularity (ΔE_{90}; dihedral angle = 90°) seen by the repetition of two transition-state geometries. The calculated barriers ΔE_0 and ΔE_{90} are 652 and 579 cm^{-1}, respectively. For the excited-state dihedral scan shown in Figure 9a, the global minimum geometry corresponds to a structure with a dihedral angle close to 90°, whereas the dihedral angle of the LE minimum geometry is near 0°. This torsional phase shift between the ground and excited electronic states leads to nuclear arrangements that may hinder or enhance electron charge transfer upon excitation as will be discussed in the Discussion section. Here, the lowest calculated barriers to interconversion are 863 cm^{-1} for the perpendicular conformation to isomerize to the planar configuration, whereas it would require 496 cm^{-1} for the planar structure to convert into the perpendicular geometry.

The ground-state 1PhPy + $1H_2O$ potential energy scan is presented in Figure S1, showing different torsional barriers than 1PhPy. In particular for the ground state, ΔE_0 = 1033 cm^{-1}, whereas ΔE_{90} is significantly reduced to 174 cm^{-1}. The torsional potential energy surface for 1PhPy + $1H_2O$ in the excited state changes drastically compared to the bare 1PhPy chromophore. Strikingly, ΔE_0 = 2371 cm^{-1}, which is twice the energy than in the ground state, and there is no longer a barrier to perpendicularity. Similar figures displaying the torsional potential energy surfaces of 1PhPy + $2H_2O$ and 1PhPy + $3H_2O$ in both the ground and excited states can be found in the Supporting Information (Figures S4 and S5). As will be discussed in the Discussion section, the addition of water significantly changes the preferred conformation, photophysics, and the degree to which intramolecular charge transfer occurs upon photoexcitation.

Experimental Results. The first 700 cm^{-1} of the resonant two-photon ionization (R2PI) spectrum for 1-phenylpyrrole (1PhPy) is shown in Figure 3. The electronic origin band located at 35 490 cm^{-1} is similar to that reported by Okuyama and Thomas.[25,26] Upon closer inspection of the R2PI

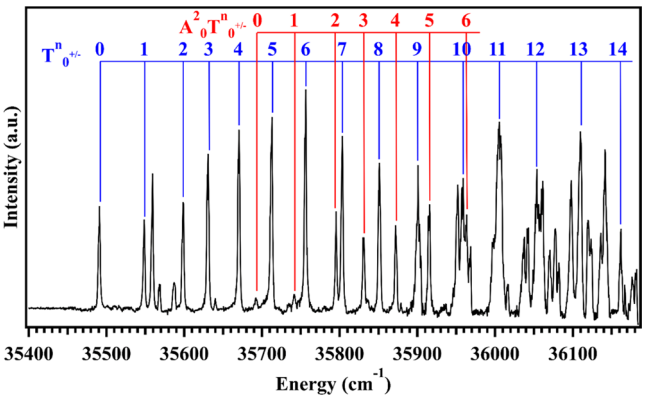

Figure 3. R2PI spectrum of 1-phenylpyrrole (1PhPy). The blue trace signifies transitions due to the torsional mode progression ($T^n_{0^{+/-}}$), and the red trace indicates the $A^2_0T^n_{0^{+/-}}$ band progression with mixed vibrational mode character.

spectrum, a regular ~50 cm^{-1} spacing between vibronic transitions is built off the origin, in addition to further vibronic activity at higher energy. The vibronic peaks with ~50 cm^{-1} spacing is likely due to the torsion vibrational mode between the pyrrole and phenyl rings as observed in previous studies.[25,26] Okuyama et al. originally assigned alternating excited-state vibronic bands with even quanta due to torsional transitions from v'' = 0 to v' = 0, 2, 4, etc. (e.g., T^n_0, n = even), while also assigning odd number quanta to torsional transitions with v'' = 1 to v' = 1, 3, 5, etc. (e.g., T^n_1, n = odd). More recently, the rotationally resolved spectroscopy measurements recorded by Thomas et al. provided evidence that the torsional transitions originated from v'' = 0 since the rotational constants remained the same for each transition. According to the calculated dihedral potential energy surface shown in Figure 9b, the torsional barriers for 1PhPy are sufficiently large such that the low-lying torsional energy levels will occur in degenerate pairs. For example, the T_{0^+} and T_{0^-} levels are degenerate but have vibrational wavefunctions that are symmetric and antisymmetric, respectively, with respect to the planar configuration. The selection rules governing the observed vibronic transitions dictate that the vibrational wave function has the same symmetry with respect to torsion in both the ground and excited electronic states. Therefore, the label $T^n_{0^{+/-}}$ indicates the series of transitions $T^0_{0^+}$, $T^1_{0^-}$, $T^2_{0^+}$, $T^3_{0^-}$, etc.

We, therefore, reassign the peaks with a ~50 cm^{-1} spacing between adjacent vibronic bands to both even and odd quanta in the torsional mode ($T^n_{0^{+/-}}$) as originating from v'' = 0. Additionally, the 50 cm^{-1} torsional progression is in better agreement with the calculated torsional mode for the bent structure (T = 47 cm^{-1}) in the excited electronic state compared to the higher-energy LE isomer (T = 88 cm^{-1}). The vibronic peaks labeled blue in Figure 3 represent the progression with increasing quanta placed in the excited-state torsional mode from v'' = 0, $T^n_{0^{+/-}}$. As predicted from calculations, the geometry change between the ground and excited electronic states is expected to be large, giving rise to a long Franck−Condon intensity profile.

As previously mentioned, there is a significant change in geometry between the ground and excited electronic states of 1PhPy. Not only does the torsion dihedral shift, but the excited-state calculations point to a geometry that is bent with the pyrrole ring oriented toward the phenyl ring. Therefore, vibrational modes reflecting this geometry change may

https://doi.org/10.1021/acs.jpca.2c00585
J. Phys. Chem. A 2022, 126, 4313−4325

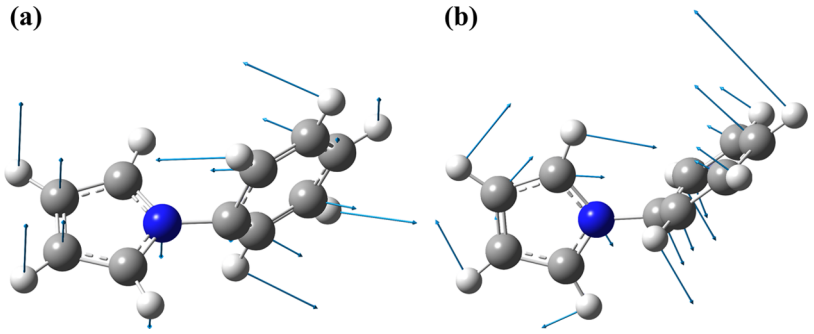

Figure 4. (a) Twisting-like and (b) bending vibrational modes of 1PhPy with arrows displaying the relative magnitudes of nuclear displacement. Calculations were performed at the TD-DFT ωB97X-D/6-311G++(d,p) level of theory.

plausibly be activated and observed in the electronic spectrum. The second progression labeled red in the R2PI spectrum in Figure 3 was mentioned in the work by Okuyama et al., but the authors did not make an assignment of the possible vibrational mode. We assign this progression (labeled $A_0^2T_{0^{+/-}}^n$) to a combination band involving the torsional mode, $T_{0^{+/-}}^n$, with another type of nuclear motion since the spacing between vibronic peaks is approximately 50 cm^{-1}. The energy difference between the electronic origin band and the beginning of the $A_0^2T_{0^{+/-}}^n$ progression is approximately 200 cm^{-1}. However, there are no fundamental vibrational modes with frequencies that closely match this energy difference from theoretical calculations. Alternatively, there are two low-frequency modes shown in Figure 4 that are in good agreement with the onset of this progression when given two quanta. The A mode may belong to a twisting-like motion between the two aromatic rings (Figure 4) with a calculated frequency of 101 cm^{-1}. Here, this twisting-like vibrational mode has a″ symmetry in the C_s point group since its motion is perpendicular to the symmetry plane. The overall symmetry of the vibronic wavefunctions must be totally symmetric to be observed in the R2PI spectrum, which is accomplished with an even number of quanta in the A vibrational mode. The observed transitions in the progression would then be $A_0^2T_{0^+}^0$, $A_0^2T_{0^-}^1$, $A_0^2T_{0^+}^2$, $A_0^2T_{0^-}^3$, etc. Another possible assignment of the $A_0^2T_{0^{+/-}}^n$ progression may involve the torsional mode combined with a bending-like motion between the pyrrole and phenyl rings shown in Figure 4, with a predicted frequency at 80 cm^{-1}. Activation of this vibrational mode is consistent with the large geometry change between the ground and excited electronic states, wherein the pyrrole ring is oriented toward the phenyl aromatic ring. With two quanta along this bending-like mode, the predicted vibronic band would be in close agreement with the observed beginning of the $A_0^2T_{0^{+/-}}^n$ progression. To obtain the correct overall symmetry, the progression would similarly be $A_0^2T_{0^+}^0$, $A_0^2T_{0^-}^1$, $A_0^2T_{0^+}^2$, $A_0^2T_{0^-}^3$, etc. The remaining weak features below 35 650 cm^{-1} are tentatively assigned as either A_0^1 vibrational modes or A_0^1T combination bands.

Although ion signal was observed in the 1PhPy + $1H_2O$ mass channel, no resonant transitions were recorded when the probe wavelength was scanned. However, when water was entrained in the supersonic jet expansion, new transition bands were found in the R2PI spectrum of 1PhPy (top black trace in Figure 5) at longer wavelengths when monitoring the 1PhPy mass ion signal. We, therefore, used ultraviolet holeburning (UVHB) to separate and assign vibronic features due to individual isomers. The middle trace (labeled red) in the figure shows the holeburning spectrum due to 1PhPy when the

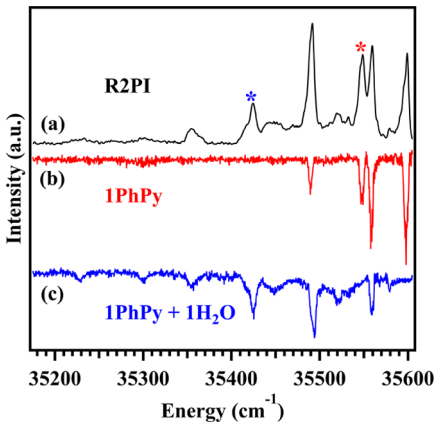

Figure 5. (a) R2PI spectrum recorded while monitoring the 1PhPy (m/z = 143) mass channel when water is entrained in the gas expansion. (b) Holeburn spectrum assigned to the bare 1PhPy chromophore obtained when the holeburn laser is resonant on the vibronic transition labeled with a red asterisk in the R2PI spectrum. (c) Holeburn spectrum assigned to the 1PhPy + $1H_2O$ complex when the holeburn laser is resonant on the new vibronic transition labeled with a blue asterisk in the R2PI spectrum.

holeburn laser is resonant on the transition in the R2PI spectrum labeled with a red asterisk. However, when the holeburn laser is resonant with the new vibronic peak labeled with a blue asterisk, we obtain the holeburning spectrum shown in the bottom of the figure (blue trace). Since there are no other predicted isomers of 1PhPy, we assign these new vibronic features to the 1PhPy + $1H_2O$ molecular complex decomposing to $1PhPy^+$ and water fragments following photoionization. The low-energy van der Waals interaction (hydrogen atom-π) between 1PhPy and water is likely exceeded upon ionization of the molecular complex. We observe the same holeburning spectrum shown in the bottom of Figure 5 when the holeburn laser is resonant with the other new bands not assigned to 1PhPy, albeit with a smaller signal-to-noise ratio. No ion signal in the mass spectrum could be observed for higher-order water complexes with 1PhPy that would indicate larger complexes decomposing into the $1PhPy^+$ mass channel; typical concentrations of water entrained in the gas expansion was ∼0.05%. Furthermore, these new vibronic features disappear under warmer supersonic expansion conditions, indicating they are not due to 1PhPy "hot bands." The 1PhPy + $1H_2O$ vibronic spectrum is shown in Figure 6 with tentative assignments for the observed transitions. Similar to the bare 1PhPy chromophore, we observe regular spacing between the new vibronic transitions

https://doi.org/10.1021/acs.jpca.2c00585
J. Phys. Chem. A 2022, 126, 4313−4325

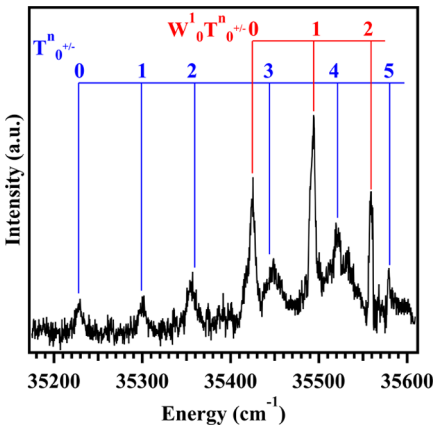

Figure 6. Vibronic spectrum of the 1PhPy + $1H_2O$ complex. The new vibronic features are assigned to the torsional modes $T^n_{0^{+/-}}$ (blue tie lines) and the water-migration $W^1_0T^n_{0^{+/-}}$ combination band (red tie lines) of 1PhPy + $1H_2O$.

of approximately 70 cm^{-1}, which we assign to increasing quanta placed in the torsional mode, $T^n_{0^{+/-}}$.

The electronic origin band is assigned to the lowest-energy peak observed at 35 227 cm^{-1}, which is red-shifted from the 1PhPy bare chromophore origin by 263 cm^{-1}. The intermolecular interaction of water with 1PhPy can be best described as a weak Coulombic attraction (water binds as a proton donor to the aromatic rings) rather than a true hydrogen bond. Thus, the relative stabilization of this interaction is reflected in the modest redshift of the 1PhPy + $1H_2O$ electronic origin band with respect to 1PhPy. Additionally, the weak interaction between 1PhPy and water may also explain the likely fragmentation of the 1PhPy + $1H_2O$ complex upon photoionization, arising as new resonant features observed in the 1PhPy R2PI spectrum. The vibronic spectrum of 1PhPy + $1H_2O$ does not extend as far in energy with regards to the R2PI spectrum of 1PhPy, likely due to the dissociation of the molecular complex to fragments. From the spectrum, we speculate that the dissociation energy of 1PhPy + $1H_2O$ is approximately the energy difference between the electronic origin band and the last vibronic transition, ~350 cm^{-1}. We note that this value is lower than the calculated binding energy by about a factor of six (~2000 cm^{-1} depending on if zero-point effects are taken into account).

As shown in Figure 6, the 1PhPy + $1H_2O$ vibronic peaks have been assigned in a similar manner to that in the R2PI spectrum of 1PhPy. The transitions labeled blue in the figure have a spacing of approximately 70 cm^{-1}, which we assign to the torsional mode, $T^n_{0^{+/-}}$ having a calculated vibrational frequency of 74 cm^{-1} in the excited state. As shown in the upper panel of Figure S1, the 1PhPy + $1H_2O$ torsional potential energy surface in the excited state displays a barrier to planarity that is larger by a factor of two compared to the bare 1PhPy chromophore (Figure 9b). The increased torsional frequency is consistent with a roughly 2-fold heightening of the torsional barrier predicted for 1PhPy + $1H_2O$. Furthermore, the observed ~70 cm^{-1} progression is in excellent agreement with calculations predicting a torsional vibrational mode of 74 cm^{-1}.

In contrast to the 1PhPy R2PI spectrum, the vibronic band progression beginning at 196 cm^{-1} above the electronic origin is significantly more intense than the torsional progression in the R2PI spectrum of 1PhPy + $1H_2O$. As indicated from our calculated results in Figure 2 (and in more detail in Figure S10), the water solvent migrates from the pyrrole ring to the phenyl ring upon electronic excitation, following the electron charge transfer. Thus, one anticipates large Franck−Condon activity in modes due to the water structural reorganization. As shown in Figure 7, two water-migration modes calculated at 149 and 159 cm^{-1} have been identified that are in fair agreement with the onset of the vibronic band progression. Indeed, much of the nuclear displacement is due to the single H_2O molecule translation, with some displacement along the aromatic ring bending coordinate. We therefore assign the vibronic band progression (red trace) starting at 196 cm^{-1} to a combination of the water-migration and torsional modes of 1PhPy + $1H_2O$, labeled $W^1_0T^n_{0^{+/-}}$.

DISCUSSION

Simulation of Vibronic Spectra with 1D DVR Calculations. The DVR calculations can be thought of as a more numerical approach to interpreting the spectra, which we can use to complement the interpretations and insights given above in the experimental section.

1PhPy + $1H_2O$ Spectrum. We begin our discussion with the 1PhPy + $1H_2O$ complex due to its simpler spectral structure. The fitted potential energy surfaces used in the DVR calculations (with energy levels in black) are shown in Figure 8a. The results for the fitted spectrum (described below) are shown in Figure 8b. Two models for the potential energy surface were considered: (1) the first model fits the torsional potential of the ground and excited states to the electronic energy obtained after a constrained optimization of all of the other coordinates and (2) the second model calculates is an

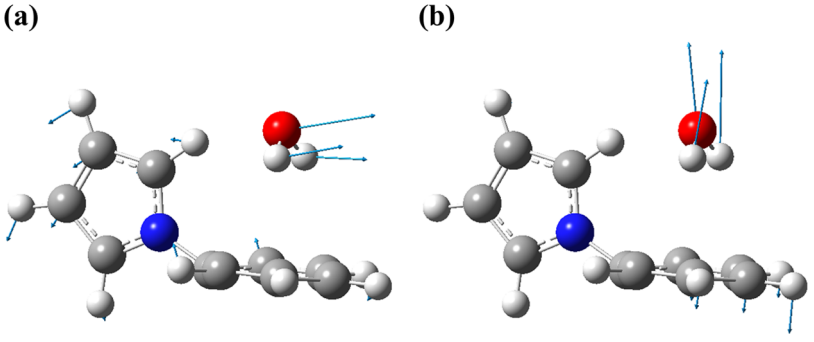

Figure 7. (a, b) Water-migration vibrational modes of 1PhPy + $1H_2O$ with arrows displaying the relative magnitudes of nuclear displacement. Calculations were performed at the TD-DFT ωB97X-D/6-311G++(d,p) level of theory.

https://doi.org/10.1021/acs.jpca.2c00585
J. Phys. Chem. A 2022, 126, 4313−4325

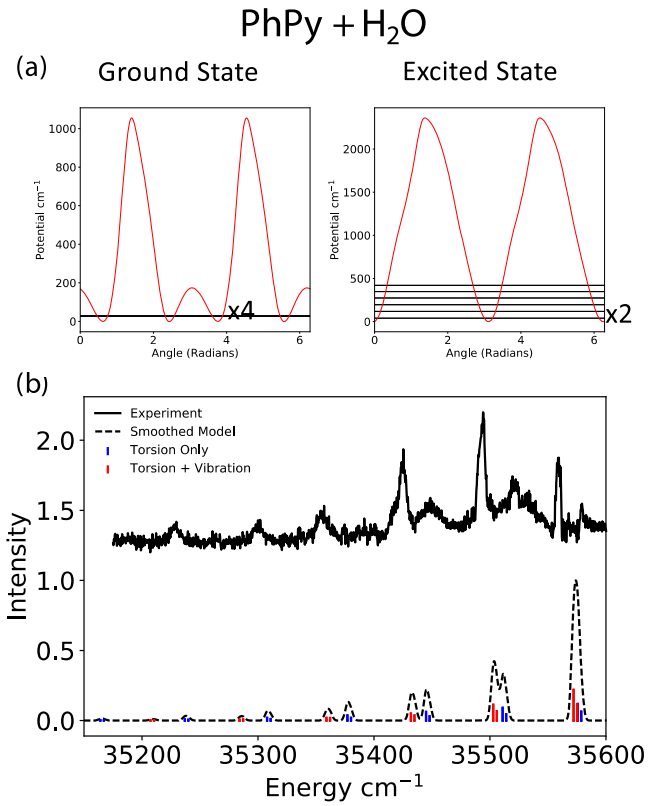

Figure 8. (a) Interpolated torsional potential energy surfaces for the 1PhPy + $1H_2O$ complex. The horizontal lines are the calculated energy levels from the 1D DVR calculations. The x4 on the ground state indicates that there are four states close to each other in energy (as x2 does for the excited state, where they are doubly degenerate). (b) Calculated spectrum for the 1PhPy + $1H_2O$ complex plotted against the experimental spectrum. Details are provided in the main text.

unrelaxed scan about the torsion (Supporting Figures). The first model, with constrained optimization, is used in Figure 8 (and 9 for 1PhPy). The spectra resulting from the other model are provided in the Supporting Information (Figure S6). The energies and wavefunctions were calculated under the periodic formulation of the DVR method on both the ground and excited states.[38] Relative intensities are found from the squared magnitude of the overlap integrals from the ground-state torsional wavefunctions and the excited-state wavefunctions. The ground-state torsional potential has four lowest-energy states within 2 cm^{-1} of each other, and all four are used as potential initial states when generating pairs of ground-state potentials with the excited torsional states.

Though both the excited-state and ground-state masses are, in principle, tunable parameters, the spectrum is only sensitive to the excited-state mass as the quartet of states on the ground state are close to each other (the fitted ground and excited masses are 120.2 and 115.2 amu, respectively).

As discussed above, the addition of considering transitions that involve a second vibrational mode is necessary to fully model the spectrum—this shift is set to 195 cm^{-1}, and the peaks that result from these transitions are shown in red. Peaks that result from purely torsional transitions are modeled in blue. Making the first sharp peak the origin of a second transition fits better over the entire 35 400−35 600 cm^{-1} range. In general, the model appears to underestimate the relative intensities of the first few transitions, but overall, the fitting captures the relative growth of the spectral intensities of each progression over the observed spectral interval. The progression that is offset by 195 cm^{-1} has its estimated intensities multiplied by 6.0, as this seemed to improve the agreement between relative integrated intensities of the two progressions in the 35 400−35 600 cm^{-1} range.

A closer look at the wavefunctions and energies of the numerical results can help with the interpretation of the spectrum. The ground-state torsional surface has an alternating (high to low) structure in the barrier to rotation, which when plotted over one full period resembles a double-well of double-well structure. Since the lower barrier is still over 150 cm^{-1}, this potential structure or a torsional problem with such a high mass results in the ground state being nearly quadruply degenerate, as expected above. The excited-state torsional surface only has two barriers every period, and this results in the states being nearly numerically doubly degenerate pairs (within 10^{-6} cm^{-1}).

The largest overlaps between the torsional wavefunctions occur between the third torsional state on the ground-state surface and the 26th torsional state on the excited-state surface (a full list of the state overlaps is given in the Supporting Information Github repo as .csv files). However, there are states with appreciable overlaps all the way up to the 40th torsional state (which is calculated to be at ∼1400 cm^{-1}). The observed torsional progression is significantly shorter than the predicted one, which could be a consequence of diminishing photoionization efficiency owing, for example, to the dissociation of water from the complex.

One compromise that this implementation of the DVR approach has comes from the perspective of interpretability. The grid is defined on a semiopen interval (with the end point fixed at 360°), but even at high numbers of grid points, there is an asymmetry on the end points. This leads to the final wavefunctions as calculated with the DVR method being localized to individual wells, and thus, we do not obtain eigenstates states that map directly onto the 0^- and 0^+ state interpretation given above, though approximate linear combinations could be taken, as has been done for the dihedral coordinates. The higher symmetry of the single water complex and the uncomplexed PhPy systems provide challenges that might not be observed in larger complexes with less symmetry. In these cases where the torsional potentials have more features, the grid-based approaches would be able to deal with these complicated potentials without having as many complications of higher symmetry.

1PhPy Spectrum. The fitted ground- and excited-state surfaces of the model spectrum of 1PhPy are shown in Figure 9a. For this molecule, the simplified 1D DVR picture is not able to capture all of the experimentally observed features. Specifically, the progression is predicted to continue to much higher energies than experimentally observed.

We again find a periodic double well of double-well potential for the ground state, which results in the lowest four states forming a quartet on the ground-state potential energy surface (however, the barriers are much closer in height as opposed to the complexed case). Unlike with the 1PhPy + $1H_2O$ complex, we do not have a reason to terminate the progression of the overlaps at lower energies. Thus, the spectrum under this simple one-dimensional model is expected to progress much longer than is experimentally observed. To understand these effects, it is likely necessary to account for dynamical effects or potentially higher-dimensional calculations would be needed.

https://doi.org/10.1021/acs.jpca.2c00585
J. Phys. Chem. A 2022, 126, 4313−4325

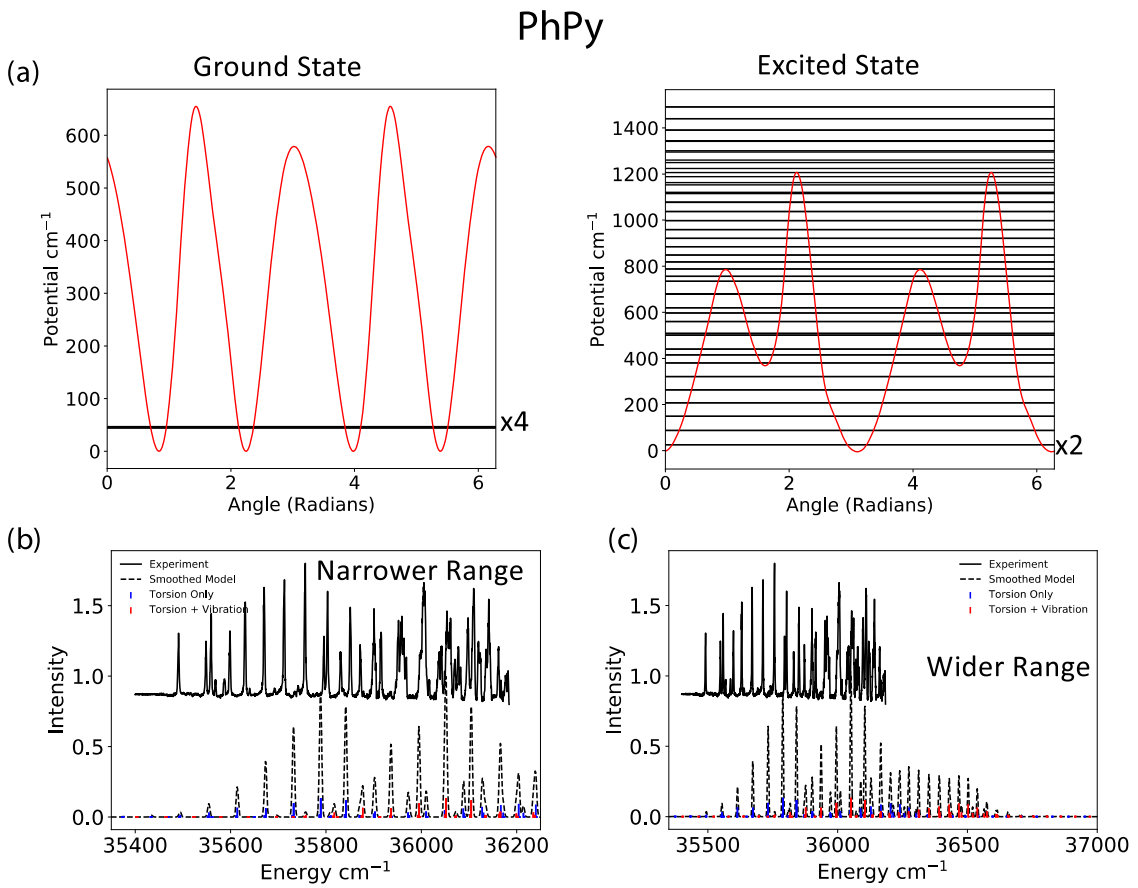

Figure 9. (a) Interpolated torsional potential energy surfaces and lower-energy DVR energy levels for the 1PhPy molecule. (b, c) Calculated spectrum for the 1PhPy molecule plotted against the experimental spectrum, for narrower (b) and wider ranges (c), respectively.

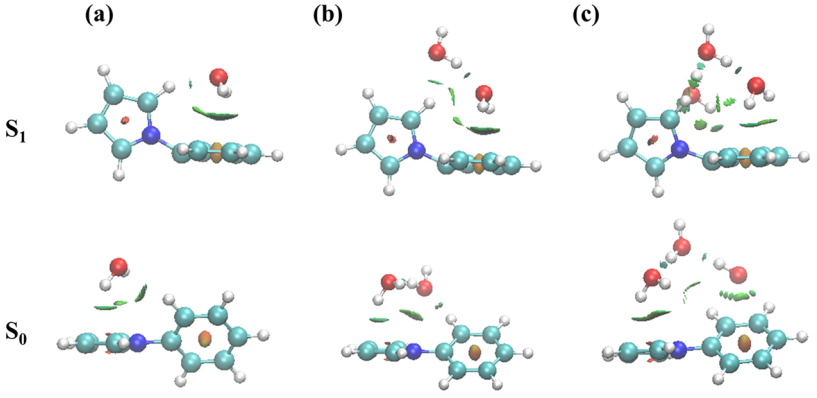

Figure 10. Noncovalent interactions and accompanying isosurfaces for both ground and excited states of (a) 1PhPy + 1H_2O, (b) 1PhPy + 2H_2O, and (c) 1PhPy + 3H_2O. Blue and green identify hydrogen-bonding (strong attraction, blue) and van der Waals interactions (weak attraction, green). Red indicates repulsive interactions.

Despite these shortcomings, the approximate spacing and structure in the spectrum are reproducible through the same procedure employed in fitting the PhPy + 1H_2O spectrum.

Noncovalent Interactions within Water-Solvated 1-Phenylpyrrole Complexes. To facilitate the interpretation of the intermolecular interactions present within the 1PhPy + nH_2O complexes, we performed a noncovalent interaction (NCI) analysis using NCIPLOT.[39] This method investigates the electron density regions, in which the reduced density gradient (RDG; $s(\rho)$) vanishes at low electron densities. The NCI analysis provides isosurfaces to visualize the RDG in regions far from the nuclei, where intermolecular interactions manifest themselves through singularities of the electron density. The sign of the second Hessian eigenvalue (λ_2) of the electronic density ρ distinguishes between different types of noncovalent interactions. The strength of the interaction can be derived from ρ in the corresponding region, which is color-coded with blue signifying strong hydrogen bonding, green representing weak van der Waals attraction, and red indicating strong repulsive interaction.

The 1PhPy geometries and extended hydrogen-bonding networks with water solvation shown in Figure 2 can be better understood by analyzing their respective intermolecular interactions. Figure 10 summarizes the NCI isosurfaces

https://doi.org/10.1021/acs.jpca.2c00585
J. Phys. Chem. A 2022, 126, 4313−4325

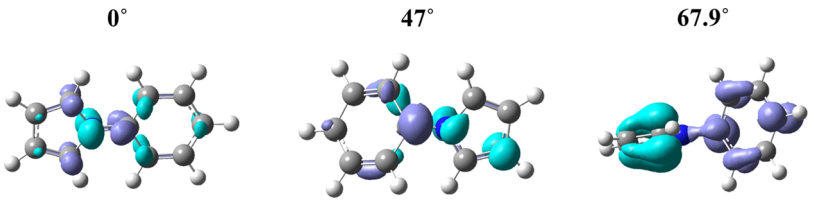

Figure 11. Electron density difference maps revealing the charge transfer for 1PhPy at different CN−CC dihedral angles in the excited electronic state. Cyan indicates the initial electron density in the highest occupied molecular orbital (HOMO), and purple represents the final density shift to the lowest unoccupied molecular orbital (LUMO) after excitation.

imprinted on the ground- and excited electronic-state geometries of 1PhPy + nH$_2$O, n = 1−3. In general, water acts as a reporter of the charge localization on the pyrrole or phenyl aromatic ring in the ground and excited electronic states. As can be seen in the figure, the water molecules have a propensity to interact with the pyrrole π orbital in the ground state, whereas water prefers to bind with the phenyl π^* orbital upon excitation of 1PhPy. In particular, the dominant interaction of the single water with 1PhPy in the ground state involves weak van der Waals attractions between the water hydrogen atoms with the pyrrole aromatic ring as indicated by the green isosurfaces. These weak interactions increase with two and three water molecules solvating 1PhPy, where the water network eventually bridges the pyrrole and phenyl rings for 1PhPy + 3H$_2$O. Furthermore, stronger hydrogen-bonding type interactions are observed between water molecules. As a result of the water hydrogen-bonding network accommodating 1PhPy via weak hydrogen/van der Waals interactions, the CN−CC dihedral of 1PhPy in the molecular complexes changes appreciably from the bare 1PhPy chromophore.

Upon $\pi\pi^*$ excitation of 1PhPy with the electron charge now localized on the phenyl ring, stabilization of the charge distribution is accomplished by a reorganization of the water hydrogen-bonding network (see Figure S8). More specifically, the upper panel of Figure 10 illustrates water's key role in facilitating charge transfer between the pyrrole and phenyl aromatic rings. Indeed, the water network is increasingly stabilizing the nuclear geometry of the 1PhPy chromophore into a more perpendicular orientation. With the addition of a single water molecule, a weak attractive interaction is present between the water hydrogen atoms and the phenyl ring π^* orbital, in addition to a stronger hydrogen bond between the oxygen atom of water and the pyrrole ring C−H bond. Therefore, the bent perpendicular geometry of 1PhPy within the complex is more stabilized compared with the bare 1PhPy chromophore. This geometrical change is also supported by the agreement of the DVR simulations of the complexed structure with the experimental observations. This is consistent with the barrier to perpendicularity decreasing for the 1PhPy + 1H$_2$O excited electronic state shown in Figures 8 and S2. As the water network grows, the weak stabilizing attractions with the pyrrole ring steer the 1PhPy geometry toward a CN−CC dihedral angle approaching ∼90°. Therefore, the NCI analysis reveals that upon sequential water molecule solvation of 1PhPy, the lower-energy twisted intramolecular charge transfer (TICT) geometry is obtained. The charge transfer dynamics and fluorescence emission outcomes of 1PhPy with an increasingly polar solvation environment are the focus of the next section.

Twisted Intramolecular Charge Transfer Dynamics of 1-Phenylpyrrole. Visualizing the movement of charge that occurs when a molecular chromophore is excited is useful when understanding the TICT geometry of 1PhPy. To this end, calculations were carried out to obtain electron density difference maps for several dihedral angles of interest for the bare 1PhPy chromophore illustrated in Figure 11. Cyan indicates the areas of electron depletion within 1PhPy, while purple shows the areas of electron density gain upon excitation from the ground to excited electronic state. As shown in the figure, charge transfer appears to redistribute from the pyrrole group to the phenyl ring in most conformations of 1PhPy, except when the dihedral angle approaches planarity which is at an energetic maximum. 1PhPy shows minimal charge transfer for the higher-energy isomer with a partially twisted geometry (47°) and for geometries possessing planar dihedral angles (0 or 180°). However, charge transfer from the pyrrole ring donor to the phenyl ring acceptor is significant when 1PhPy adopts the lowest-energy bent configuration (TICT geometry) with a dihedral angle of 67.9°.

Since solvent interactions were predicted to increase the likelihood of TICT,[27,40] we expect different photophysical behavior for 1PhPy when it complexes with water. As seen in Figure S1, the ground-state barrier to perpendicularity (ΔE_{90}) is much lower for 1PhPy + 1H$_2$O than the 1PhPy bare chromophore. The ΔE_{90} difference is even more striking as revealed in the 1PhPy + 1H$_2$O excited-state potential energy scan results. With the addition of a single water molecule, there is no ΔE_{90} for the 1PhPy + 1H$_2$O complex. In fact, the nearly perpendicular conformation is the lowest-energy geometry with barriers located at planarity (0 and 180°). The agreement between the R2PI spectrum and the DVR simulations for 1PhPy + 1H$_2$O further indicates a substantial decrease in energy for ΔE_{90}, supporting that TICT is enhanced with water solvation. Close inspection of the 1PhPy + 1H$_2$O electron density difference maps in Figure 12 show that charge transfer is evident at all of the dihedral angle conformations, particularly when the 1PhPy chromophore in the complex resembles the bent TICT geometry with a CN−CC dihedral angle closer to 90°. These results indicate that water solvent intermolecular interactions are extremely important in facilitating the TICT configuration for 1PhPy.

To further explore the importance of water solvation in facilitating TICT in 1PhPy, we carried out analogous calculations for 1PhPy + nH$_2$O (n = 2, 3). Figure 12 also shows that charge transfer occurs for 1PhPy + 2H$_2$O at all dihedral angles, even for planar and perpendicular geometries. Additionally, 1PhPy + 3H$_2$O continues this trend, where conformations with CN−CC dihedral angles at 0, 90, and 180° show charge transfer is facilitated by the water solvation network. This result is reflected in the dihedral potential energy surfaces (see Figures S3 and S4 in the Supporting Information), where a more perpendicular TICT geometry is

https://doi.org/10.1021/acs.jpca.2c00585
J. Phys. Chem. A 2022, 126, 4313−4325

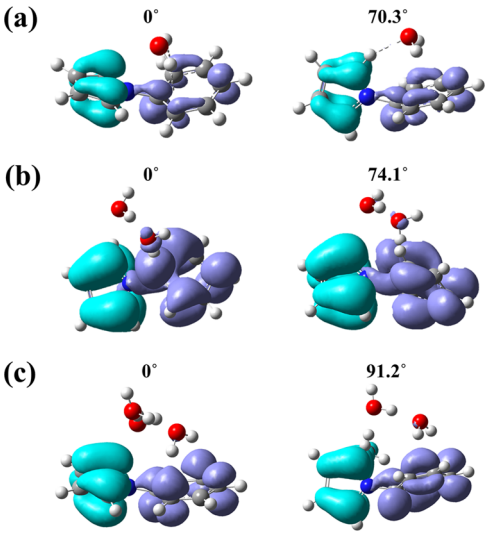

Figure 12. Electron density difference maps revealing the charge transfer for (a) 1PhPy + $1H_2O$, (b) 1PhPy + $2H_2O$, and (c) 1PhPy + $3H_2O$ at different CN−CC dihedral angles in the excited electronic state. Cyan indicates the initial electron density in the HOMO and purple represents the final density shift to the LUMO after excitation.

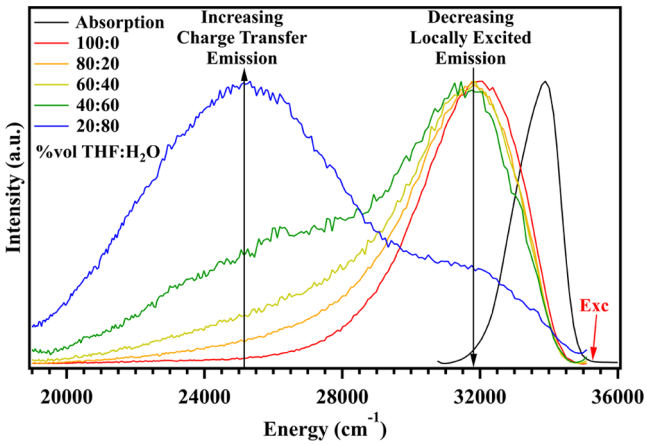

Figure 13. Absorption and fluorescence spectra of 1-phenylpyrrole in tetrahydrofuran (THF) with increasing % volume of water (H_2O) at 25 °C. In 100% volume THF, the fluorescence spectrum consists of emission from a locally excited (LE) state. As the % volume H_2O increases, the fluorescence spectra display decreasing relative emission intensity from the LE state and increasing emission from the twisted intramolecular charge transfer (TICT) state. The excitation wavelength used during experiments was 280 nm.

also the lowest-energy excited-state conformation for 1PhPy + nH_2O (n = 2, 3).

As observed from the electron density difference map results, the polar water solvation environment stabilizes the excited-state TICT geometry, acquiring an increasingly perpendicular CN−CC dihedral and less strained NCC angle with the size of the hydrogen-bonding network. Previous theoretical and experimental studies on the fluorescence of 1PhPy in different nonpolar and polar solvents have demonstrated dual emission bands.[23,24,29] These studies rationalized the red-shifted emission feature appearing in acetonitrile as a signature of 1PhPy undergoing torsional isomerization from the locally excited (LE) electronic-state configuration to the more stabilized TICT geometry. Radiative relaxation from the excited-state TICT configuration to the ground electronic state is therefore often referred to as the charge transfer emission band and is observed at a lower fluorescence energy.

To connect our gas-phase 1PhPy + nH_2O complex studies to the water-aqueous environment surrounding brown carbon (BrC) chromophores within aerosols, we obtained the absorption and fluorescence spectra of 1PhPy in nonpolar tetrahydrofuran (THF) solvent with an increasing % volume of water. Figure 13 shows the absorption spectrum (black trace) of 1PhPy in 100% volume THF. Using 280 nm (35 714 cm^{-1}) as the excitation wavelength, we obtained the corresponding fluorescence spectrum in 100% volume THF showing a single emission band at ∼32 000 cm^{-1} resulting from the LE state in relatively nonpolar solvents. As a greater % volume H_2O is incorporated into the samples, the appearance of the second TICT emission band is observed at approximately 25 000 cm^{-1} with a concomitant decrease in intensity of the LE band. Therefore, with increasingly polar water solvation environments surrounding 1PhPy chromophores, the results indicate that emission from the excited-state TICT geometry becomes dominant for larger concentrations of water. This is consistent with the 1PhPy + nH_2O results, wherein water directly facilitates a TICT geometry from which the signature emission band is observed at a lower energy in the fluorescence spectra. Aguilar and co-workers[29] reported the optimized geometries and energetics in the ground, LE, and TICT electronic states in the gas phase and in acetonitrile solution. 1PhPy adopted a preferred TICT geometry in acetonitrile, wherein emission to the ground state explained the charge transfer emission band in polar solvents. They concluded that the TICT state is stabilized, and its energy becomes similar to the LE minimum. Therefore, the dual fluorescence was attributed to the TICT geometry accessible in polar solvents due to the free energy surface being very flat, making emission possible from any point along the path from the LE state to the TICT state.

CONCLUSIONS

To develop a better understanding of the photophysics of a prototypical chromophore in brown carbon (BrC) aerosols, we explored the local solvation intermolecular interactions of 1PhPy with H_2O. The present study on 1PhPy + nH_2O clusters (n = 0−3) has provided a molecular-scale picture of the charge transfer dynamics of 1PhPy with and without the presence of water. Using a combination of experimental and theoretical approaches, we determined that H_2O plays an active role in facilitating the structural orientation and thus the charge transfer efficacy of 1PhPy. Spectroscopic assignments for 1PhPy and 1PhPy + $1H_2O$ have been made using mass-resolved double-resonance spectroscopies and interpreted using 1-dimensional discrete variable representation (1D DVR) simulations. Progressions in the torsional mode ($T^n_{0^{+/-}}$) are observed in the excited-state spectra of 1PhPy and 1PhPy + $1H_2O$, in which the spacings between transitions are ∼50 and 70 cm^{-1}, respectively. Furthermore, either the bending or twisting-like nuclear motions couple with the torsional mode, yielding the other $A^2_0T^n_{0^{+/-}}$ progression in the R2PI spectrum of 1PhPy. Water migration upon excitation activates Franck−Condon modes observed in the 1PhPy + $1H_2O$ R2PI spectrum, indicating a structural reorganization of the water network responding to the charge transfer. Indeed, the spectroscopy reveals that the intermolecular interactions with H_2O result in 1PhPy preferring a twisted intramolecular charge

https://doi.org/10.1021/acs.jpca.2c00585
J. Phys. Chem. A 2022, 126, 4313−4325

transfer (TICT) geometry. The sequential binding of H_2O to 1PhPy stabilizes the TICT geometry with a CN−CC dihedral that is nearly perpendicular, facilitating charge transfer from the pyrrole π orbital donor to the phenyl π^* orbital acceptor. Predictions from analysis of the noncovalent interactions and electron density different maps upon photoexcitation further support that the local H_2O environment mediates the charge transfer within 1PhPy by reorganizing the hydrogen-bonding network. Measurements from condensed-phase experiments agree with the gas-phase results, whereby we observe greater fluorescence emission from the TICT geometry of 1PhPy as the concentration of H_2O is increased.

■ ASSOCIATED CONTENT

Supporting Information

The Supporting Information is available free of charge at https://pubs.acs.org/doi/10.1021/acs.jpca.2c00585.

Electronic potential energy surfaces for 1PhPy and 1PhPy + $1H_2O$, 1D DVR simulations of spectra on unrelaxed potential energy surfaces, and example plots of calculated torsional wavefunctions (PDF)

■ AUTHOR INFORMATION

Corresponding Authors

Daniel P. Tabor − *Department of Chemistry, Texas A&M University, College Station, Texas 77843, United States;* orcid.org/0000-0002-8680-6667; Email: daniel_tabor@tamu.edu

Nathanael M. Kidwell − *Department of Chemistry, The College of William and Mary, Williamsburg, Virginia 23187-8795, United States;* orcid.org/0000-0002-7065-4486; Email: nmkidwell@wm.edu

Authors

Brianna N. Peterson − *Department of Chemistry, The College of William and Mary, Williamsburg, Virginia 23187-8795, United States*

Megan E. Alfieri − *Department of Chemistry, The College of William and Mary, Williamsburg, Virginia 23187-8795, United States*

David J. Hood − *Department of Chemistry, The College of William and Mary, Williamsburg, Virginia 23187-8795, United States;* orcid.org/0000-0002-5895-9690

Christian D. Hettwer − *Department of Chemistry, The College of William and Mary, Williamsburg, Virginia 23187-8795, United States*

Daniel V. Costantino − *Department of Chemistry, The College of William and Mary, Williamsburg, Virginia 23187-8795, United States;* orcid.org/0000-0002-0177-7992

Complete contact information is available at: https://pubs.acs.org/10.1021/acs.jpca.2c00585

Notes

The authors declare no competing financial interest.

■ ACKNOWLEDGMENTS

This material is based upon work supported by the National Science Foundation to N.M.K. under Grant No. CHE-2102501. Partial support of this research from the Commonwealth Center for Energy and the Environment is also gratefully acknowledged by B.N.P., M.E.A., D.J.H., C.D.H., D.V.C., and N.M.K. N.M.K. also acknowledges William & Mary Research Computing for providing computational resources that contributed to the results reported within this paper. D.P.T. acknowledges support from Texas A&M University startup funding and the Robert A. Welch Foundation (Grant No. A-2049-20200401). Portions of this research were conducted with high-performance research computing resources provided by Texas A&M University HPRC.

■ REFERENCES

(1) Xantheas, S. S.; Voth, G. A. Aqueous Solutions and Their Interfaces. *J. Phys. Chem. B* **2009**, *113*, 3997−3999.

(2) Rodgers, J. M.; Weeks, J. D. Interplay of Local Hydrogen-Bonding and Long Ranged Dipolar Forces in Simulations of Confined Water. *Proc. Natl. Acad. Sci. U.S.A.* **2008**, *105*, 19136−19141.

(3) Cheung, M. S.; Garcia, A. E.; Onuchic, J. N. Protein Folding Mediated by Solvation: Water Expulsion and Formation of the Hydrophobic Core Occur After the Structural Collapse. *Proc. Natl. Acad. Sci. U.S.A.* **2002**, *99*, 685−690.

(4) Zhuravlev, P. I.; Papoian, G. A. Functional Versus Folding Landscapes: The Same Yet Different. *Curr. Opin. Struct. Biol.* **2010**, *20*, 16−22.

(5) Onuchic, J. N.; Wolynes, P. G. Theory of Protein Folding. *Curr. Opin. Struct. Biol.* **2004**, *14*, 70−75.

(6) Hoff, A. J.; Deisenhofer, J. Photophysics of Photosynthesis. Structure and Spectroscopy of Reaction Centers of Purple Bacteria. *Phys. Rep.* **1997**, *287*, 1−247.

(7) Magnuson, A.; Anderlund, M.; Johansson, O.; Lindblad, P.; Lomoth, R.; Polivka, T.; Ott, S.; Stensjo, K.; Styring, S.; Sundstrom, V.; Hammarström, L. Biomimetic and Microbial Approaches to Solar Fuel Generation. *Acc. Chem. Res.* **2009**, *42*, 1899−1909.

(8) LeBard, D. N.; Matyushov, D. V. Energetics of Bacterial Photosynthesis. *J. Phys. Chem. B* **2009**, *113*, 12424−12437.

(9) Bianchi, F.; Tröstl, J.; Junninen, H.; Frege, C.; Henne, S.; Hoyle, C. R.; Molteni, U.; Herrmann, E.; Adamov, A.; Bukowiecki, N.; et al. New Particle Formation in the Free Troposphere: A Question of Chemistry and Timing. *Science* **2016**, *352*, 1109−1112.

(10) Bzdek, B. R.; DePalma, J. W.; Johnston, M. V. Mechanisms of Atmospherically Relevant Cluster Growth. *Acc. Chem. Res.* **2017**, *50*, 1965−1975.

(11) Bzdek, B. R.; Reid, J. P. Aerosol Microphysics: From Molecules to the Chemical Physics of Aerosols. *J. Chem. Phys.* **2017**, *147*, No. 220901.

(12) Tabor, D. P.; Kusaka, R.; Walsh, P. S.; Sibert, E. L.; Zwier, T. S. Isomer-Specific Spectroscopy of Benzene-(H2O) n, n = 6,7: Benzene's Role in Reshaping Water's Three-Dimensional Networks. *J. Phys. Chem. Lett.* **2015**, *6*, 1989−1995.

(13) Headrick, J. M.; Diken, E. G.; Walters, R. S.; Hammer, N. I.; Christie, R. A.; Cui, J.; Myshakin, E. M.; Duncan, M. A.; Johnson, M. A.; Jordan, K. D. Spectral Signatures of Hydrated Proton Vibrations in Water Clusters. *Science* **2005**, *308*, 1765−1769.

(14) Pachauri, R. K.; Allen, M. R.; Barros, V. R.et al. *Climate Change 2014: Synthesis Report. Contribution of Working Groups I, II and III to the Fifth Assessment Report of the Intergovernmental Panel on Climate Change*; Pachauri, R. K.; Meyer, L. A., Eds.; IPCC: Geneva, Switzerland, 2014; p 151.

(15) Lary, D. J.; Lee, A. M.; Toumi, R.; Newchurch, M. J.; Pirre, M.; Renard, J. B. Carbon Aerosols and Atmospheric Photochemistry. *J. Geophys. Res.: Atmos.* **1997**, *102*, 3671−3682.

(16) Chung, S. H.; Seinfeld, J. H. Global Distribution and Climate Forcing of Carbonaceous Aerosols. *J. Geophys. Res.: Atmos.* **2002**, *107*, AAC 14-1−AAC14-33.

(17) Andreae, M. O.; Gelencsér, A. Black Carbon or Brown Carbon? The Nature of Light-Absorbing Carbonaceous Aerosols. *Atmos. Chem. Phys.* **2006**, *6*, 3131−3148.

(18) Carslaw, K. S.; Lee, L. A.; Reddington, C. L.; Pringle, K. J.; Rap, A.; Forster, P. M.; Mann, G. W.; Spracklen, D. V.; Woodhouse, M. T.;

Regayre, L. A.; Pierce, J. R. Large Contribution of Natural Aerosols to Uncertainty in Indirect Forcing. *Nature* **2013**, *503*, 67−71.
(19) McCoy, I. L.; McCoy, D. T.; Wood, R.; Regayre, L. A.; Watson-Parris, D.; Grosvenor, D. P.; Mulcahy, J. P.; Hu, Y.; Bender, F. A. M.; Field, P. R.; et al. The Hemispheric Contrast in Cloud Microphysical Properties Constrains Aerosol Forcing. *Proc. Natl. Acad. Sci. U.S.A.* **2020**, *117*, 18998−19006.
(20) Lin, G.; Penner, J. E.; Flanner, M. G.; Sillman, S.; Xu, L.; Zhou, C. Radiative Forcing of Organic Aerosol in the Atmosphere and on Snow: Effects of SOA and Brown Carbon. *J. Geophys. Res.: Atmos.* **2014**, *119*, 7453−7476.
(21) Laskin, A.; Laskin, J.; Nizkorodov, S. A. Chemistry of Atmospheric Brown Carbon. *Chem. Rev.* **2015**, *115*, 4335−4382.
(22) Phillips, S. M.; Smith, G. D. Light Absorption by Charge Transfer Complexes in Brown Carbon Aerosols. *Environ. Sci. Technol. Lett.* **2014**, *1*, 382−386.
(23) Yoshihara, T.; Druzhinin, S. I.; Zachariasse, K. A. Fast Intramolecular Charge Transfer with a Planar Rigidized Electron Donor/Acceptor Molecule. *J. Am. Chem. Soc.* **2004**, *126*, 8535−8539.
(24) Yoshihara, T.; Druzhinin, S. I.; Demeter, A.; Kocher, N.; Stalke, D.; Zachariasse, K. A. Kinetics of Intramolecular Charge Transfer with N-Phenylpyrrole in Alkyl Cyanides. *J. Phys. Chem. A* **2005**, *109*, 1497−1509.
(25) Okuyama, K.; Numata, Y.; Odawara, S.; Suzuka, I. Electronic Spectra of Jet-Cooled 1-Phenylpyrrole: Large-Amplitude Torsional Motion and Twisted Intramolecular Charge-Transfer Phenomenon. *J. Chem. Phys.* **1998**, *109*, 7185.
(26) Thomas, J. A.; Young, J. W.; Fleisher, A. J.; Alvarez-Valtierra, L.; Pratt, D. W. Stark-Effect Studies of 1-Phenylpyrrole in the Gas Phase. Dipole Reversal upon Electronic Excitation. *J. Phys. Chem. Lett.* **2010**, *1*, 2017−2019.
(27) Proppe, B.; Merchán, Manuela.; Serrano-Andrés, L. Theoretical Study of the Twisted Intramolecular Charge Transfer in 1-Phenylpyrrole. *J. Phys. Chem. A* **2000**, *104*, 1608−1616.
(28) Manz, J.; Proppe, B.; Schmidt, B. Time-Resolved Dual Fluorescence of 1-Phenylpyrrole in Acetonitrile: Molecular Dynamics Simulations of Solvent Response to Twisted Intramolecular Charge Transfer. *Phys. Chem. Chem. Phys.* **2002**, *4*, 1876−1881.
(29) Fdez Galván, I.; Martín, M. E.; Muñoz-Losa, A.; Sánchez, M. L.; Aguilar, M. A. Solvent Effects on the Structure and Spectroscopy of the Emitting States of 1-Phenylpyrrole. *J. Chem. Theory Comput.* **2011**, *7*, 1850−1857.
(30) Schweke, D.; Haas, Y.; Dick, B. Photophysics of Phenylpyrrole Derivatives and Their Acetonitrile Clusters in the Gas Phase and in Argon Matrixes: Simulations of Structure and Reactivity. *J. Phys. Chem. A* **2005**, *109*, 3830−3842.
(31) Pan, C.; Zhang, Y.; Lee, J. D.; Kidwell, N. M. Imaging the Dynamics of CH2BrI Photodissociation in the Near Ultraviolet Region. *J. Phys. Chem. A* **2018**, *122*, 3728−3734.
(32) Frisch, M. J.; Trucks, G. W.; Schlegel, G. W.; Scuseria, G. E.; Robb, M. A.; Cheeseman, J. R.; Scalmani, G.; Barone, V.; Petersson, G. A.; Nakatsuji, H.et al. *Gaussian 16*, Revision C.01; Gaussian Inc.: Wallingford CT, 2016.
(33) Chai, J. D.; Head-Gordon, M. Long-Range Corrected Hybrid Density Functionals with Damped Atom-Atom Dispersion Corrections. *Phys. Chem. Chem. Phys.* **2008**, *10*, 6615−6620.
(34) Chai, J. D.; Head-Gordon, M. Systematic Optimization of Long-Range Corrected Hybrid Density Functionals. *J. Chem. Phys.* **2008**, *128*, No. 084106.
(35) Rohrdanz, M. A.; Martins, K. M.; Herbert, J. M. A Long-Range-Corrected Density Functional That Performs Well for Both Ground-State Properties and Time-Dependent Density Functional Theory Excitation Energies, Including Charge-Transfer Excited States. *J. Chem. Phys.* **2009**, *130*, No. 054112.
(36) Zhang, J.; Dolg, M. ABCluster: The Artificial Bee Colony Algorithm for Cluster Global Optimization. *Phys. Chem. Chem. Phys.* **2015**, *17*, 24173−24181.
(37) Korn, J. A.; Tabor, D. P.; Sibert, E. L.; Zwier, T. S. Conformation-Specific Spectroscopy of Alkyl Benzyl Radicals: Effects of a Radical Center on the CH Stretch Infrared Spectrum of an Alkyl Chain. *J. Chem. Phys.* **2016**, *145*, No. 124314.
(38) Colbert, D. T.; Miller, W. H. A Novel Discrete Variable Representation for Quantum Mechanical Reactive Scattering via the S-matrix Kohn Method. *J. Chem. Phys.* **1992**, *96*, 1982.
(39) Contreras-García, J.; Johnson, E. R.; Keinan, S.; Chaudret, R.; Piquemal, J.-P.; Beratan, D. N.; Yang, W. NCIPLOT: A Program for Plotting Noncovalent Interaction Regions. *J. Chem. Theory Comput.* **2011**, *7*, 625−632.
(40) Sasaki, S.; Drummen, G. P. C.; Konishi, G. Recent Advances in Twisted Intramolecular Charge Transfer (TICT) Fluorescence and Related Phenomena in Materials Chemistry. *J. Mater. Chem. C* **2016**, *4*, 2731−2743.

Recommended by ACS

Solvent Effect on Excited-State Intramolecular Proton-Coupled Charge Transfer Reaction in Two Seven-Membered Ring Pyrrole-Indole Hydrogen Bond Systems
Min Tao, Andong Xia, *et al.*
SEPTEMBER 29, 2021
THE JOURNAL OF PHYSICAL CHEMISTRY B
READ

Gas-Phase Fluorescence of Proflavine Reveals Two Close-Lying, Brightly Emitting States
Iden Djavani-Tabrizi and Rebecca A. Jockusch
MARCH 01, 2022
THE JOURNAL OF PHYSICAL CHEMISTRY LETTERS
READ

Illuminating Excited-State Intramolecular Proton Transfer of a Fungi-Derived Red Pigment for Sustainable Functional Materials
Taylor D. Krueger, Chong Fang, *et al.*
DECEMBER 23, 2021
THE JOURNAL OF PHYSICAL CHEMISTRY C
READ

The Ultrafast Quantum Dynamics of Photoexcited Adenine–Thymine Basepair Investigated with a Fragment-based Diabatization and a Linear Vibronic...
Martha Yaghoubi Jouybari, Fabrizio Santoro, *et al.*
OCTOBER 05, 2021
THE JOURNAL OF PHYSICAL CHEMISTRY A
READ

Get More Suggestions >

https://doi.org/10.1021/acs.jpca.2c00585
J. Phys. Chem. A 2022, 126, 4313−4325